

Article

# Removal of Emerging Contaminants from Water by Using Carbon Materials Derived from Tingui Shells

Débora dos Santos <sup>1,\*</sup>, Wardleison Moreira <sup>1</sup>, Thiago de Araújo <sup>2</sup>, Maria Bernardo <sup>3,\*</sup>, Isabel Fonseca <sup>3</sup>,  
Indianara Ostroski <sup>4</sup> and Maria Angélica de Barros <sup>1</sup>

<sup>1</sup> Department of Chemical Engineering, State University of Maringá, Maringá 87020-900, PR, Brazil; wmmoreira@uem.br (W.M.); masdbarros@uem.br (M.A.d.B.)

<sup>2</sup> Department of Chemical Engineering, Federal Technological University of Paraná, Ponta Grossa 84017-220, PR, Brazil; thiago@flashrg.com.br

<sup>3</sup> Associated Green Chemistry Laboratory (LAQV) of the Chemistry and Technology Network (REQUIMTE), Department of Chemistry, NOVA School of Science and Technology, NOVA University Lisbon, 2829-516 Caparica, Portugal; blo@fct.unl.pt

<sup>4</sup> Institute of Chemistry, Federal University of Goiás, Goiânia 74690-900, GO, Brazil; indianara\_ostroski@ufg.br

\* Correspondence: deborafederici37@gmail.com (D.d.S.); maria.b@fct.unl.pt (M.B.)

**Abstract:** This study explored the adsorption of acetaminophen and caffeine using CO<sub>2</sub>-activated biochar (BT-CO<sub>2</sub>) and hydrochar (HT-CO<sub>2</sub>) derived from Tingui shell biomass. The experimental data from kinetic and equilibrium adsorption tests were employed in batch and fixed-bed systems. In the batch system, a specific amount of the adsorbent was added to a known volume of the solution, and the mixture was agitated for a set period to allow adsorption to occur. In the fixed-bed system, the solution was passed through a column packed with the adsorbent, allowing for continuous adsorption. These systems pave the way for future research. The findings revealed that HT-CO<sub>2</sub> exhibited a greater surface area and a higher presence of oxygen-containing functional groups than BT-CO<sub>2</sub>. These functional oxygen groups had a notable impact on the adsorption capacity of the adsorbents for pharmaceutical substances. In the batch systems, BT-CO<sub>2</sub> demonstrated a maximum adsorption capacity of 221.4 mg g<sup>-1</sup> for acetaminophen and 162.7 mg g<sup>-1</sup> for caffeine, while HT-CO<sub>2</sub> exhibited higher capacities of 383.2 mg g<sup>-1</sup> for acetaminophen and 189.7 mg g<sup>-1</sup> for caffeine. In the fixed bed configuration, HT-CO<sub>2</sub> displayed a maximum adsorption capacity of 82.2 mg g<sup>-1</sup> for acetaminophen and 45.60 mg g<sup>-1</sup> for caffeine. The predominant mechanisms involved in the removal of acetaminophen and caffeine were identified as H-bonding and  $\pi$ - $\pi$  bonds. These results underscore the promising potential of these carbons as effective adsorbents for treating water contaminated with pharmaceutical residues, inspiring further exploration in this field and offering hope for the future of water treatment by providing a solid foundation for future research and development.

**Keywords:** pyrolysis; hydrocarbonization; CO<sub>2</sub>-activation; pharmaceuticals; aquatic environment



**Citation:** dos Santos, D.; Moreira, W.; de Araújo, T.; Bernardo, M.; Fonseca, I.; Ostroski, I.; de Barros, M.A.

Removal of Emerging Contaminants from Water by Using Carbon Materials Derived from Tingui Shells. *Separations* **2024**, *11*, 215. <https://doi.org/10.3390/separations11070215>

Academic Editor: Hongbo Gu

Received: 17 June 2024

Revised: 4 July 2024

Accepted: 10 July 2024

Published: 12 July 2024



**Copyright:** © 2024 by the authors. Licensee MDPI, Basel, Switzerland. This article is an open access article distributed under the terms and conditions of the Creative Commons Attribution (CC BY) license (<https://creativecommons.org/licenses/by/4.0/>).

## 1. Introduction

Acetaminophen and caffeine are pharmaceutical agents widely used in human and veterinary medicine. Acetaminophen, categorized as an analgesic and antipyretic, is renowned for alleviating pain and reducing fever. It is widely used to treat mild to moderate pain, including headaches, muscle aches, and fever typically associated with viral or bacterial infections [1]. In contrast, caffeine stands out as a central nervous system stimulant. It is widely recognized for improving alertness, attention, and cognitive function and is often used to combat fatigue [2].

Due to their extensive use, acetaminophen and caffeine are often found in water matrices [3] as a consequence of human consumption and subsequent excretion, as well as the improper disposal of medicines [4]. This raises significant environmental concerns since these compounds come into contact with living beings in the receiving waters. They

can cause adverse changes in aquatic organisms' endocrine, immune, and reproductive systems [5]. This highlights the urgent need for effective waste management and water treatment policies and practices to mitigate the negative impacts of these emerging contaminants. The detection and quantification of acetaminophen and caffeine in aquatic environments are essential for assessing the extent of contamination and developing strategies to protect the health of marine ecosystems and, by extension, public health.

Traditional water and wastewater treatment technologies often prove ineffective in removing emerging contaminants, such as pharmaceutical compounds, requiring more efficient alternatives or improvements to existing ones [6]. One of those approaches is adsorption, which has stood out as a highly effective technique for removing pharmaceutical residues from water, mainly using highly efficient, cost-effective, and novel eco-friendly adsorbents [7].

The search for adsorbents with the properties mentioned above has been an essential focus of the scientific community, and biomass-derived carbons have been successfully explored as adsorbents of emerging drugs from the aquatic environment [7–9]. Using biomass wastes as precursors of carbon-based adsorbents provides a sustainable disposal option for those wastes, with the advantages of low cost and huge availability. Biomass-derived carbons can be produced by different carbonization methods, such as hydrothermal carbonization (HTC) and conventional pyrolysis. Engineered biochar (BC) and hydrochar (HC) have garnered considerable attention among researchers as alternative adsorbents aiming to replace traditional activated carbons [8,10].

The *Magonia pubescent* St. Hil. tree, known in Brazil as Tingui, is widely distributed in the vast Cerrado area (Brazilian savannah), with its fruits and seeds used for the preparation of soaps and extraction of a wide range of bioactive compounds with applications in medicine [11–13]. This abundance of Tingui shells, which are currently discarded, presents a significant opportunity for valorization. Previous works have studied the conversion of Tingui shell biochars into porous carbons through chemical activation with KOH and ZnCl<sub>2</sub>, followed by an application as an adsorbent of pharmaceutical compounds, with excellent results [14,15]. This study aimed to further explore the potential of Tingui shells by generating activated biochar and hydrochar from them, thereby demonstrating this sustainable resource's promising potential in waste management and water treatment, instilling a sense of optimism in the audience about the future of these fields.

This study aimed to generate activated biochar and hydrochar from Tingui fruit shells. In the present manuscript, both biochars and hydrochars were submitted for CO<sub>2</sub> activation. The obtained activated carbons were applied to remove acetaminophen and caffeine from water samples in batch and fixed-bed systems. A comprehensive physicochemical characterization was conducted on the produced carbon materials to understand better their structural and chemical properties and their performance in removing the pharmaceutical compounds from water. The obtained data is crucial for the development of more effective adsorbent materials and for the advancement of contaminated water treatment technologies. Understanding the structural properties of adsorbents and their impact on the removal of pollutants makes optimizing the production and activation processes possible, thus improving the efficiency of the materials produced from Tingui fruit shells. This work's innovation lies in using different adsorbents synthesized from Tingui for the water adsorption of acetaminophen and caffeine, a novel approach that could significantly impact the water treatment field and inspire the development of more innovative solutions, inspiring the audience with the potential of this research.

## 2. Materials and Methods

### 2.1. Synthesis of Activated Biochar and Hydrochar

In pyrolysis, 75 g of Tingui shells underwent thermal decomposition in a tubular oven (model SANCHIS, 2335, Porto Alegre, RS, Brazil) at 550 °C for 120 min. The process used a heating rate of 10 °C per minute and a nitrogen flow rate of 150 mL per minute. The resulting material from this pyrolysis process was designated as biochar of Tingui

(BT). Subsequently, the BT underwent activation with carbon dioxide (CO<sub>2</sub>) within a stainless-steel reactor inside a tubular furnace, maintained at 850 °C for 120 min. This activation process, known as CO<sub>2</sub> activation, involved the exposure of the biochar to high temperatures in the presence of CO<sub>2</sub>, which led to the development of a porous structure and increased surface area, enhancing its adsorption properties. The reactor was heated at 10 °C per minute, and a CO<sub>2</sub> flow of 150 mL per minute was maintained throughout the process. The resulting material post-activation was named CO<sub>2</sub>-activated Tingui biochar (BT-CO<sub>2</sub>).

7.5 g of Tingui shells and 30 mL of distilled water were added to the autoclave reactor under limited oxygen conditions for hydrothermal carbonization. The autoclave reactor was placed in the forced circulation oven (Nova Ética, NT535) and kept at 200 °C for 1440 min, using a heating rate of 10 °C min<sup>-1</sup>. The material obtained after hydrocarbonization was called hydrochar of Tingui (HT). The HT was then activated with carbon dioxide (CO<sub>2</sub>) using the same conditions described above for BT. The material obtained after activation was called CO<sub>2</sub>-activated Tingui hydrochar (HT-CO<sub>2</sub>).

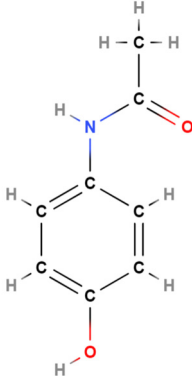
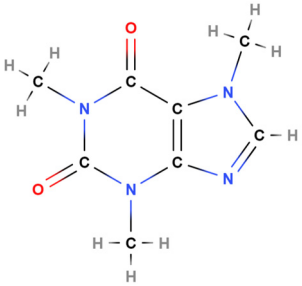
## 2.2. Textural and Chemical Characterizations of BT, BT-CO<sub>2</sub>, HT, and HT-CO<sub>2</sub>

The textural properties of BT, BT-CO<sub>2</sub>, HT, and HT-CO<sub>2</sub> samples were assessed using N<sub>2</sub> adsorption/desorption isotherms at 77 K with a Micromeritics ASAP 2020 volumetric adsorption analyzer. The Brunauer–Emmett–Teller (BET) method determined the specific surface area (S<sub>BET</sub>). The total pore volume (V<sub>p</sub>) was obtained from N<sub>2</sub> adsorption at a relative pressure (P/P<sub>0</sub>) of 0.95. The micropore volume (V<sub>micro</sub>) was calculated using the t-plot method, while the mesopore volume (V<sub>meso</sub>) was derived by subtracting V<sub>micro</sub> from V<sub>p</sub>. The average pore diameter (D<sub>p</sub>) was determined using the formula  $4V_p/S_{BET}$ . Thermogravimetric (TG) curves were acquired using a TA Instruments Discovery series thermal analyzer, model TGA 55. The samples were heated from 25 to 1000 °C at 10 °C per minute in a synthetic air atmosphere during the analysis. Raman spectra were recorded at wavelengths ranging from 400 to 4000 cm<sup>-1</sup> using a Bruker Laser Raman Spectrometer with a 532 nm laser line and a power of 20 mW. Functional groups were identified using Fourier transform infrared spectroscopy (FTIR) with the KBr pellet method (Vertex 70v, Bruker, Karlsruhe, Germany) in transmittance mode within the 400 to 4000 cm<sup>-1</sup> infrared range. Elemental analysis was performed using a Thermo Finnigan Flash EA 1112, Rodano, Italy CHNS series analyzer, and the oxygen (O) content was determined by the difference method:  $O = 100 - C - H - N - S$ . The pH at the zero charge point (pH<sub>PCZ</sub>) was determined using pH change analysis. In this process, 20 mg of the material was mixed with 50 mL of 0.1 mol L<sup>-1</sup> NaCl solution at various initial pH values (ranging from 2 to 12), adjusted with 0.1 mol L<sup>-1</sup> HCl or NaOH solutions. The pH was measured after 24 h of stirring in an orbital shaker at 150 rpm and 25 °C. A plot of the final pH versus the initial pH was then created. Ash analysis was conducted at 750 °C following the Standard Test Method—Designation: D1762–84 (Reapproved 2021). Mineral analysis of BT, BT-CO<sub>2</sub>, HT, and HT-CO<sub>2</sub> was carried out under European Standard EN 15290 (2011) [16]. For the acid digestion procedure, 50 mg of a material sample was weighed into Teflon flasks, and 12 mL of HCl and 3 mL of HNO<sub>3</sub> were added. The flasks were closed, and the mixture was subjected to microwave digestion (Milestone microwave digester, model Ethos 1600). Acid digestion was carried out initially using a power of 500 W for 15 min to reach a temperature of 190 °C, followed by a reduction in power to 400 W and a temperature of 190 °C for 20 min. Subsequently, the digests were filtered using a glass fiber filter with a porosity < 2 μm (Schleicher & Schuell, model GF/C), transferred to 100 mL flasks, and topped up with ultrapure water. The diluted digests were then analyzed by atomic absorption spectrometry (EAA equipment from Thermo Elementar Solaar, Cambridge, United Kingdom, M series, equipped with a hydride chamber from Unicam, model VP 90, Cambridge, United Kingdom). The following metals were quantified: zinc (Zn), copper (Cu), manganese (Mn), potassium (K), iron (Fe), sodium (Na), calcium (Ca), aluminum (Al), and magnesium (Mg).

### 2.3. Adsorbates

Acetaminophen and caffeine with 99% purity from Merck and Sigma-Aldrich, Missouri, United States, were quantified using UV-VIS spectrophotometry with a Hach DR 5000. The absorbance of acetaminophen was measured at 243 nm, while caffeine was measured at 273 nm. The chemical formulas and structural properties of paracetamol and caffeine are presented in Table 1.

**Table 1.** Chemical formulas and structural properties of paracetamol and caffeine.

Properties	Acetaminophen	Caffeine
Chemical formula	C <sub>8</sub> H <sub>9</sub> NO <sub>2</sub>	C <sub>8</sub> H <sub>10</sub> N <sub>4</sub> O <sub>2</sub>
pKA	9.5	14.0
Molar mass	151.17 g mol <sup>-1</sup>	194.19 g mol <sup>-1</sup>
Chemical structure		

### 2.4. Batch Adsorption Experiments

Adsorption experiments were carried out using 50 mL of acetaminophen or caffeine solutions and 20 mg of BT-CO<sub>2</sub> or HT-CO<sub>2</sub> in a batch system. The solutions were stirred at 150 rpm in a Tecnal TE-4200, Piracicaba, São Paulo, Brazil thermostatic shaker. After a specified time interval, the samples were filtered through 0.45 µm Millipore membranes and then analyzed using a Hach DR 5000 UV-VIS spectrophotometer. All samples were analyzed in duplicates.

#### 2.4.1. Adsorption Kinetics

The adsorption kinetics experiments utilized an aqueous solution with either acetaminophen or caffeine at a concentration of 100 mg L<sup>-1</sup>. The contact time between the adsorbate and the adsorbent ranged from 5 to 2880 min at a temperature of 25 °C. Equation (1) was employed to calculate the adsorption capacity of BT-CO<sub>2</sub> and HT-CO<sub>2</sub> at a specific time *t*.

$$q_t = \frac{(C_o - C_t)V}{m} \quad (1)$$

wherein  $q_t$  (mg g<sup>-1</sup>) is the amount adsorbed on the solid phase at time *t*;  $C_o$  and  $C_t$  (mg L<sup>-1</sup>) are the initial concentration of adsorbate and the concentration of adsorbate at time *t*, respectively;  $V$  (L) is the volume of the solution; and  $m$  (g) is the mass of the adsorbent material.

The experimental data derived from the adsorption kinetics were fitted to theoretical models, including the pseudo-first-order Equation (2), pseudo-second-order Equation (3), and Elovich Equation (4) models [17]:

$$q_t = q_e \left(1 - e^{-k_1 t}\right) \quad (2)$$

$$q_t = \frac{k_2 q_e^2 t}{1 + k_2 q_e t} \quad (3)$$

$$q_t = \frac{1}{\beta} \ln(1 + \alpha \beta t) \tag{4}$$

wherein  $k_1$  ( $\text{min}^{-1}$ ) is the pseudo-first-order adsorption rate constant;  $k_2$  ( $\text{min}^{-1}$ ) is the pseudo-second-order adsorption rate constant;  $\alpha$  ( $\text{mg g}^{-1} \text{min}^{-1}$ ) is the initial adsorption rate; and  $\beta$  ( $\text{mg g}^{-1}$ ) represents the desorption constant.

### 2.4.2. Adsorption Isotherms

The adsorption isotherm studies were meticulously conducted using an aqueous solution containing acetaminophen or caffeine at 25 °C. The initial concentrations of the adsorbate solution ranged from 25 to 1000  $\text{mg L}^{-1}$ . Equation (5) was employed to determine the adsorption capacity of BT-CO<sub>2</sub> or HT-CO<sub>2</sub> at equilibrium.

$$q_e = \frac{(C_0 - C_e)V}{m} \tag{5}$$

wherein  $q_e$  ( $\text{mg g}^{-1}$ ) is the amount of adsorbate adsorbed at equilibrium;  $C_0$  and  $C_e$  ( $\text{mg L}^{-1}$ ) are the initial concentration of adsorbate and the equilibrium adsorbate concentration, respectively;  $V$  (L) is the volume of the solution; and  $m$  (g) is the mass of the adsorbent material.

The experimental data collected from the adsorption isotherms were fitted to theoretical models including Langmuir Equation (6), Freundlich Equation (7), and BET Equation (8) [18]:

$$q_e = \frac{q_{max} K_L C_e}{1 + K_L C_e} \tag{6}$$

$$q_e = K_F C_e^{\frac{1}{n}} \tag{7}$$

$$q_e = \frac{q_m K_S C_e}{(1 - K_L C_e)(1 + [(K_S - K_L)C_e])} \tag{8}$$

wherein  $q_{max}$  ( $\text{mg g}^{-1}$ ) is the maximum amount of adsorbate adsorbed by the adsorbent;  $K_L$  ( $\text{L mg}^{-1}$ ) is the Langmuir adsorbate/adsorbent interaction constant;  $K_F$  ( $\text{mg}^{1-1/n} \text{L}^{1/n} \text{g}^{-1}$ ) is the Freundlich adsorption capacity constant; and  $n$  is the constant related to surface heterogeneity.  $C_e$  is the equilibrium adsorbate concentration ( $\text{mg L}^{-1}$ );  $K_S$  is the equilibrium constant of monolayer adsorption ( $\text{L mg}^{-1}$ ); and  $K_L$  is the equilibrium constant of multilayer adsorption ( $\text{L mg}^{-1}$ ).

### 2.5. Fixed Bed Column Adsorption Experiments

The fixed-bed column experiments were crucial in removing acetaminophen and caffeine from monocomponent solutions (25  $\text{mg L}^{-1}$ ) using the adsorbent with the best performance identified in the batch adsorption tests (BT-CO<sub>2</sub> or HT-CO<sub>2</sub>). These continuous system investigations were conducted in a jacketed glass column with an internal diameter of 0.5 cm and a height of 5 cm, connected to a peristaltic pump positioned at the base of the column to ensure ascending flow. In all fixed bed trials, the bed height remained constant at 2.1 cm (approximately 0.2 g of adsorbent). Temperature and flow rate were regulated at 25 °C and 3  $\text{mL min}^{-1}$ , respectively. Samples of the adsorbate were collected at the column outlet at predetermined intervals throughout the experiment to construct breakthrough curves (see Figure 1). The performance of the column was determined by calculating the breakthrough time ( $t_r$ , min), the saturation time ( $t_s$ , min), the mass transfer zone (MTZ, cm), the volume of effluent passed through the column up to the saturation point ( $V_e$ , mL), the total mass of adsorbate induced in the column up to the saturation point ( $m_{adsorbate}$ , mg), the total mass of adsorbate adsorbed by the adsorbent at the saturation point ( $m_{total}$ , mg),

the total adsorption capacity of the column ( $q_{total}$ ,  $\text{mg g}^{-1}$ ), and column removal efficiency ( $\%R$ , %) according to the Equations (9), (10), (11), (12), (13), (14), (15), and (16), respectively.

$$t_r = \frac{C}{C_0} = 0.05 \quad (9)$$

$$t_s = \frac{C}{C_0} = 0.94 \quad (10)$$

$$MTZ = h \left( 1 - \frac{t_r}{t_s} \right) \quad (11)$$

$$V_e = Q t_s \quad (12)$$

$$m_{adsorbate} = \frac{Q C_0 t_s}{1000} \quad (13)$$

$$m_{total} = \frac{Q C_0}{1000} \int_0^{t_s} \left( 1 - \frac{C_{t_s}}{C_0} \right) dt \quad (14)$$

$$q_{total} = \frac{m_{total}}{m_{adsorbent}} \quad (15)$$

$$\%R = \left( \frac{m_{total}}{m_{adsorbate}} \right) 100 \quad (16)$$

wherein  $C$  ( $\text{mg L}^{-1}$ ) is the outlet concentration;  $C_0$  ( $\text{mg L}^{-1}$ ) is the inlet concentration;  $h$  (cm) is the bed height;  $m$  (g) is the adsorbent mass; and  $Q$  ( $\text{L min}^{-1}$ ) is the volumetric flow rate.



**Figure 1.** Fixed bed schematic.

The experimental data obtained from the fixed-bed column adsorption were fitted to mathematical models including the Thomas Equation (17), Adams–Bohart Equation (18), Yoon–Nelson Equation (19), and dose–response Equation (20) models [19]:

$$\frac{C}{C_0} = \frac{1}{1 + \exp\left[\left(\frac{k_{TH}}{Q}\right)(q_0m - C_0Qt)\right]} \tag{17}$$

$$\frac{C}{C_0} = \frac{\exp(k_{AB}C_0t)}{\exp\left(\frac{k_{AB}N_0h}{v}\right) - 1 + \exp(k_{AB}C_0t)} \tag{18}$$

$$\frac{C}{C_0} = \frac{1}{1 + \exp[k_{YN}(\tau - t)]} \tag{19}$$

$$\frac{C}{C_0} = 1 - \frac{1}{1 + \left(\frac{C_0Qt}{q_0m}\right)^\alpha} \tag{20}$$

wherein  $k_{TH}$  (L mg<sup>-1</sup> min<sup>-1</sup>) is the rate constant of the Thomas model;  $q_0$  (mg g<sup>-1</sup>) is the estimated adsorption capacity;  $t$  (min) is the sampling time;  $k_{AB}$  (L mg<sup>-1</sup> min<sup>-1</sup>) is the kinetic constant of the Adams–Bohart model;  $N_0$  (mg L<sup>-1</sup>) is the maximum volumetric adsorption;  $h$  (cm) is the bed height;  $v$  (cm min<sup>-1</sup>) is the linear velocity;  $k_{YN}$  (min<sup>-1</sup>) is the rate constant of the Yoon–Nelson model;  $\tau$  (min) is the time to reach half of the inlet concentration; and  $\alpha$  (dimensionless) is the constant of the dose–response model.

### 3. Results and Discussion

#### 3.1. Physicochemical and Structural Properties of BT, BT-CO<sub>2</sub>, HT, and HT-CO<sub>2</sub>

The results of the elemental analysis of the four materials, presented in Table 2, provide significant insights. The higher carbon content of BT (71.93%) compared to HT (63.22%) is a result of the high degree of carbonization in the pyrolytic process of biomass, leading to a more condensed carbon structure. The HT sample, however, presented a much higher oxygen content (30.37%) than the BT material (18.81%), indicating higher devolatilization and deoxygenation of the Tingui shell biomass at the higher temperature used in the pyrolysis process (550 °C) than in the hydrothermal carbonization (200 °C). The higher atomic proportions of H/C and O/C in the HT sample than in BT further highlight the impact of devolatilization on the oxidation degree of the compound, resulting in lower levels of atomic proportions in the material. These insights can inspire and motivate future research in this field.

**Table 2.** Characterization parameters of the carbon materials.

Characteristics	BT	BT-CO <sub>2</sub>	HT	HT-CO <sub>2</sub>
<b>Nitrogen adsorption</b>				
S <sub>BET</sub> (m <sup>2</sup> g <sup>-1</sup> )	<5.0	239.0	30.0	485.0
V <sub>P</sub> (cm <sup>3</sup> g <sup>-1</sup> )	n.d	0.090	0.091	0.214
V <sub>microp</sub> (cm <sup>3</sup> g <sup>-1</sup> )	n.d	0.085	0.001	0.168
V <sub>mesop</sub> (cm <sup>3</sup> g <sup>-1</sup> )	n.d	0.005	0.090	0.046
<b>Elemental analysis</b>				
C (w/w %)	71.93	81.21	63.22	79.12
H (w/w %)	2.19	0.60	4.44	1.21
N (w/w %)	1.84	0.99	1.97	1.64
S (w/w %)	0.00	0.00	0.00	0.00
O (w/w %) <sup>a</sup>	18.81	14.10	30.37	16.94
H/C	0.030	0.007	0.070	0.015
O/C	0.334	0.211	0.480	0.229

Table 2. Cont.

Characteristics	BT	BT-CO <sub>2</sub>	HT	HT-CO <sub>2</sub>
<b>Ashes (w/w %)</b>				
Ash	5.23	3.10	≤1.00	1.09
<b>Zero charge point analysis</b>				
pH <sub>PCZ</sub>	5.68	5.88	6.98	7.07

$$^a \text{O (\%)} = 100 - (\text{C (\%)} + \text{H (\%)} + \text{N (\%)} + \text{S (\%)} + \text{Ash (\%)}).$$

The characterization parameters of the carbon materials, as presented in Table 2, provide a comprehensive understanding of the materials. These parameters, which include nitrogen adsorption and elemental analysis, are instrumental in interpreting the results and formulating conclusions.

In addition, it was possible to observe that both BT-CO<sub>2</sub> and HT-CO<sub>2</sub> had lower levels of hydrogen, nitrogen, and oxygen when compared to BT and HT, respectively, as a consequence of the activation process. Consequently, it was also possible to notice that the atomic ratios referring to the degree of carbonization (H/C) and the degree of hydrophobicity (O/C) of BT-CO<sub>2</sub> and HT-CO<sub>2</sub> also decreased about BT and HT, respectively.

The experimental data regarding the ash content, presented in Table 2, revealed significant differences between the materials. The ash content of both BT (5.23%) and BT-CO<sub>2</sub> (3.10%) was higher when compared to HT (≤1.00%) and HT-CO<sub>2</sub> (1.09%), respectively. The higher ash content in pyrolyzed materials is related to the increase in temperature during this process, which increases the concentration of minerals remaining in the resulting carbon. On the other hand, the lower ash content observed in the materials derived from hydrothermal carbonization may be attributed to a greater concentration of inorganic compounds dissolved in the subcritical water during the process. These findings have implications for the properties and potential applications of the materials.

Given the results obtained in the ash content analysis, only BT-CO<sub>2</sub> was analyzed for minerals, as it had the highest ash content compared to HT-CO<sub>2</sub>. It was possible to quantify K (3.08 mg g<sup>-1</sup>), Fe (0.123 mg g<sup>-1</sup>), Mg (0.043 mg g<sup>-1</sup>), and Mn (0.005 mg g<sup>-1</sup>) in BT-CO<sub>2</sub> carbon, metallic elements typically present in biomass-derived carbon.

The pH<sub>pzc</sub> values of the synthesized materials are listed in Table 2, showing no significant changes after activation. It is noted that the material carries positive charges when pH < pH<sub>pzc</sub> and negative charges when pH > pH<sub>pzc</sub> [20]. In addition, acetaminophen (pK<sub>a</sub> = 9.5) and caffeine (pK<sub>a</sub> = 14.0) were in neutral form [21,22] as the natural pH of each solution was lower than their respective pK<sub>a</sub> (pH<sub>acetaminophen</sub> = 6.01 and pH<sub>caffeine</sub> = 5.90). Thus, electrostatic interactions did not rule out the adsorption of acetaminophen and caffeine by BT-CO<sub>2</sub> and HT-CO<sub>2</sub>.

The thermogravimetric analysis of BT, BT-CO<sub>2</sub>, HT, and HT-CO<sub>2</sub> is shown in Figure 2D. All materials exhibited three distinct stages of weight loss with increasing temperature. The first stage, occurring between 25 and 200 °C, corresponds to the release of water from the materials (dehydration) [23]. Moisture loss was approximately 4.09, 0.94, 2.25, and 4.68 wt% for BT, BT-CO<sub>2</sub>, HT, and HT-CO<sub>2</sub>, respectively. The CO<sub>2</sub>-activated materials are stable at high temperatures, with losses below 10% of their mass, indicating a good potential for thermal regeneration. On the other hand, BT and HT chars presented losses of approximately 13.03 and 44.17, respectively. HT char's high mass loss is related to the low hydrothermal carbonization temperature (200 °C); thus, a high fraction of volatiles remains in the resulting char. Regarding BT char, the pyrolysis temperature of 550 °C allowed a significant devolatilization.



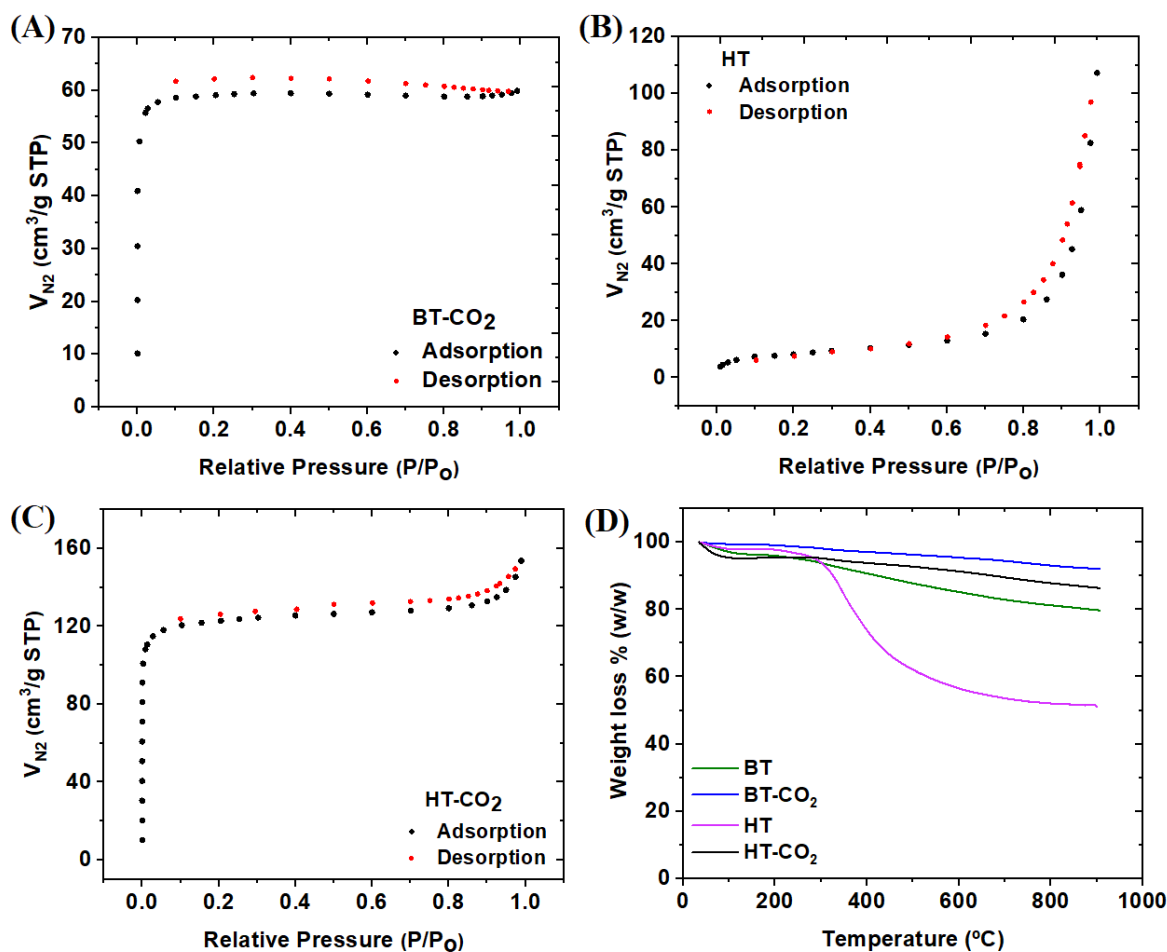


Figure 2. N<sub>2</sub> adsorption/desorption isotherms of BT-CO<sub>2</sub> (A), HT (B), and HT-CO<sub>2</sub> (C). TG of HT, HT-CO<sub>2</sub>, BT, and BT-CO<sub>2</sub> (D).

The N<sub>2</sub> adsorption/desorption isotherms of BT-CO<sub>2</sub>, HT, and HT-CO<sub>2</sub> are shown in Figure 2A, 2B, and 2C, respectively. The specific surface area ( $S_{BET}$ ), total pore volume ( $V_P$ ), micropore volume ( $V_{microp}$ ), and mesopore volume ( $V_{mesop}$ ) values for each material are presented in Table 2. The BT sample is a non-porous material (in the micro and mesopore range); thus, no isotherm was obtained. The HT exhibited a typical type IV isotherm with a type H3 hysteresis loop, indicating mesoporous characteristics with very low microporosity. Given the higher degree of devolatilization for BT char (see Figure 2D), it was expected that a more developed porosity for this char instead of hydrochar HT [10]. Hydrothermal carbonization leads to lower levels of dehydration and deoxygenation, and that is the reason why hydrochar has much more oxygen in its structure (see Table 2). The porosity development on the hydrochar might be related to the long residence time of hydrothermal carbonization (24 h) compared to the pyrolysis process (2 h), which might have privileged polymerization reactions and the formation of a char with more excellent aromatic character and structural organization [24–36].

On the other hand, BT-CO<sub>2</sub> and HT-CO<sub>2</sub> showed N<sub>2</sub> adsorption/desorption isotherms of type I (a), corresponding to microporous materials with narrow micropores [27]. The data presented in Table 2 are in accordance with what was observed in Figure 2a–c, showing that the specific surface area ( $S_{BET}$ ) and pore volume of BT and HT increased after the CO<sub>2</sub> activation process, as expected. It was also evident that HT-CO<sub>2</sub> exhibited a higher specific surface area and a larger volume of micropores than BT-CO<sub>2</sub>, probably related to the fact that the hydrochar precursor already presented a developed porosity. It is also notable in the BT-CO<sub>2</sub> isotherm, a low-pressure hysteresis likely linked to the irreversible capture of

N<sub>2</sub> molecules within pores or at pore entrances, with dimensions similar to those of the adsorbate molecule [28].

FTIR analysis was utilized to identify and characterize the functional groups present on material surfaces. Figure 3A presents the FTIR spectra of BT and BT-CO<sub>2</sub>, while Figure 3B displays the spectra of HT and HT-CO<sub>2</sub>. Regarding the FTIR spectra of BT and BT-CO<sub>2</sub>, oxygen groups were observed, indicated by the stretching vibration of the -OH group in the bands detected between 3200 and 3600 cm<sup>-1</sup> (a) [29]. The peak at 1590 cm<sup>-1</sup> (b) is associated with the vibration of C=O or C=N bonds in organic compounds [30]. At 1390 cm<sup>-1</sup> (c), it refers to the asymmetric C-H stretching of methyl [31]. The peak at 1100 cm<sup>-1</sup> (d) can be attributed to C=C stretching in aromatic groups and C-O stretching in -OCH<sub>3</sub> groups. The peaks between 850 and 600 cm<sup>-1</sup> ((e), (f), (g), and (h)) are derived from C-H bonds in aromatic rings [32]. The FTIR spectra of HT and HT-CO<sub>2</sub> showed that both materials had the same functional groups as BT and BT-CO<sub>2</sub>, with the addition of others such as C-H stretching at 2900 cm<sup>-1</sup> (i), -O-H bending at 1250 and 1200 cm<sup>-1</sup> ((j) and (k)), and C-O stretching at 1000 cm<sup>-1</sup> (l) [24]. The more significant number of oxygenated functional groups in HT compared to BT aligns with the elemental analysis results shown in Table 2, as HT-CO<sub>2</sub> (16.94%) had a higher oxygen content than BT-CO<sub>2</sub> (14.10%). Hydroxyl groups increase the polarity of the adsorbent material's surface, enhancing its affinity for various substances.

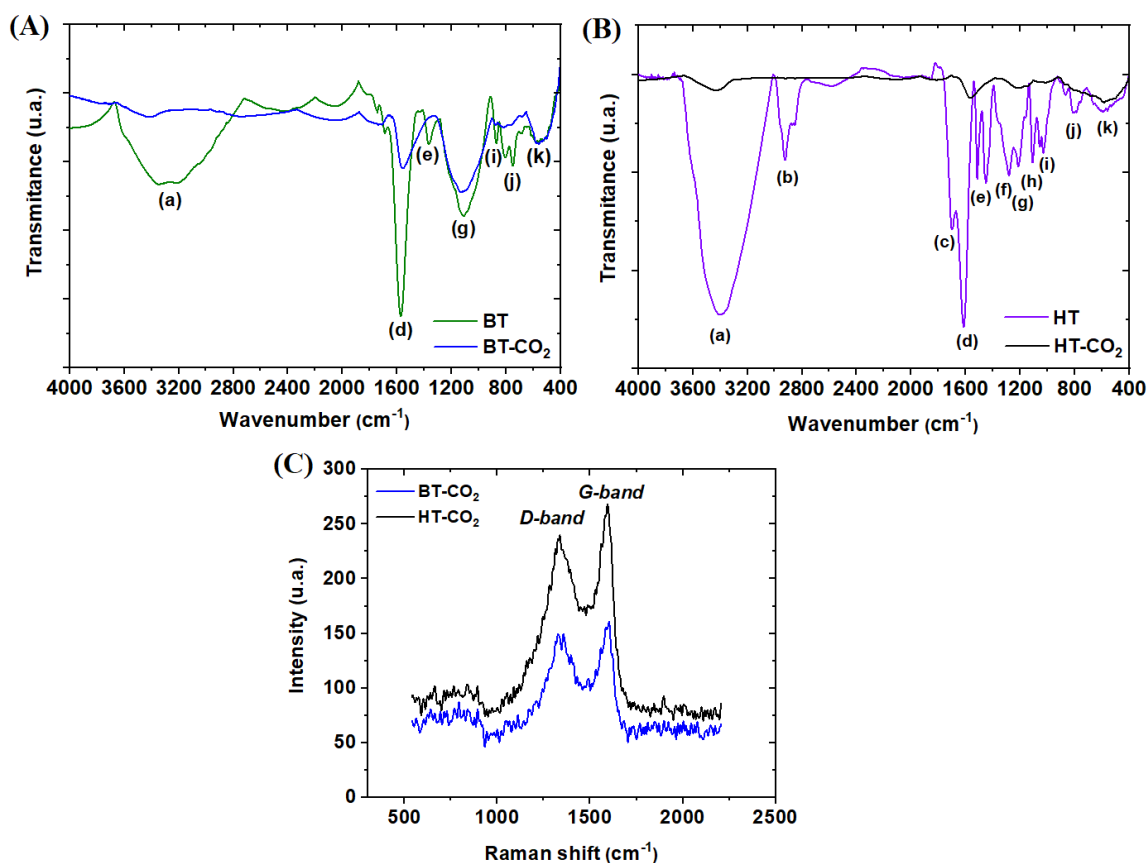


**Figure 3.** FTIR spectra of BT and BT-CO<sub>2</sub> (A) and HT and HT-CO<sub>2</sub> (B). Micro-Raman spectra of HT-CO<sub>2</sub> and BT-CO<sub>2</sub> (C).

Raman spectroscopy analysis was performed to evaluate the defects in the carbon structure and the degree of graphitization of BT-CO<sub>2</sub> and HT-CO<sub>2</sub>, as shown in Figure 3C. The peak observed at 1355 cm<sup>-1</sup> corresponds to the D band, while the peak at 1600 cm<sup>-1</sup> corresponds to the G band for BT-CO<sub>2</sub> and HT-CO<sub>2</sub>. Additionally, the ratio of the intensities of the D and G bands ( $I_D/I_G$ ) indicates the degree of disorder and graphitization

of the adsorbent. BT-CO<sub>2</sub> exhibited an I<sub>D</sub>/I<sub>G</sub> ratio of 0.933, whereas HT-CO<sub>2</sub> showed a ratio of 0.867. A higher I<sub>D</sub>/I<sub>G</sub> ratio indicates the formation of amorphous carbon adsorbents, whereas a lower ratio suggests adsorbents with more ordered structures and higher graphitization [33].

### 3.2. Batch Adsorption Kinetics

The experimental data from the adsorption kinetics tests of acetaminophen and caffeine using BT-CO<sub>2</sub> and HT-CO<sub>2</sub> are depicted in Figure 4A and 4B, respectively. It is evident that both BT-CO<sub>2</sub> and HT-CO<sub>2</sub> exhibited rapid adsorption capacities for acetaminophen and caffeine initially, but after 540 min, the rates decreased. Ultimately, equilibrium was reached around 1440 min, where the  $q_t$  values stabilized at approximately 60.8 and 94.7 mg g<sup>-1</sup> for acetaminophen using BT-CO<sub>2</sub> and HT-CO<sub>2</sub>, respectively. The adsorption capacities for caffeine in aqueous solution were 33.4 and 63.0 mg g<sup>-1</sup> for BT-CO<sub>2</sub> and HT-CO<sub>2</sub>, respectively.

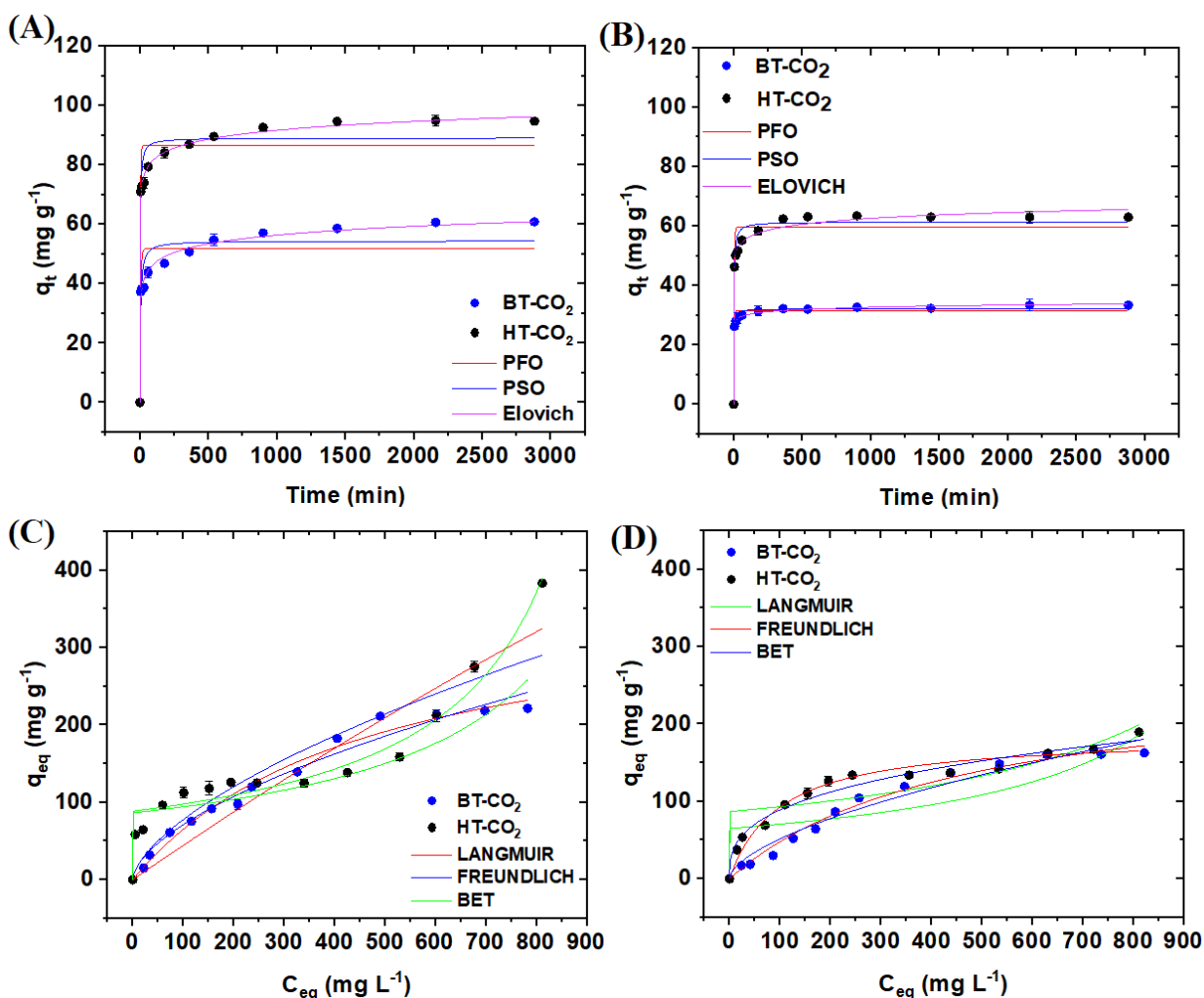


**Figure 4.** Adsorption kinetics of acetaminophen (A) and caffeine (B) by BT-CO<sub>2</sub> and HT-CO<sub>2</sub> (m = 20 mg, V = 50 mL, C = 100 mg L<sup>-1</sup>, T = 25 °C). Adsorption isotherm of acetaminophen (C) and caffeine (D) by BT-CO<sub>2</sub> and HT-CO<sub>2</sub> (m = 20 mg, V = 50 mL, C = 25–1000 mg L<sup>-1</sup>, T = 25 °C, t = 600 min).

This study employed three kinetic models—pseudo-first-order, pseudo-second-order, and Elovich—to analyze the experimental data obtained from the adsorption kinetics tests. The parameters derived from these models are presented in Table 3. The analysis of these

parameters indicates that the Elovich model best fits the experimental data, achieving a coefficient of determination ( $R^2$ ) of  $\geq 0.990$ . The Elovich model assumes that the adsorption process by the adsorbent is controlled by its chemical surface. Thus, this model assumes that the adsorption process may have been governed by chemisorption [34]. Furthermore, the high  $\alpha$  values of this model indicate that the chemical sorption strength was of the order of HT-CO<sub>2</sub> (7417.6) being greater than BT-CO<sub>2</sub> (2503.6) for acetaminophen removal. This same behavior was observed for caffeine removal, where the chemical sorption strength of HT-CO<sub>2</sub> (98,117.3) was also higher than BT-CO<sub>2</sub> (18,237.3). The low values of  $\beta$  ( $\leq 0.933$ ) indicate that BT-CO<sub>2</sub> and HT-CO<sub>2</sub> properly adsorbed these two drugs, and there was no desorption effect during the experimental process [35].

**Table 3.** Adsorption kinetics modeling parameters of BT-CO<sub>2</sub> and HT-CO<sub>2</sub>.

Model	Parameter	Acetaminophen		Caffeine	
		BT-CO <sub>2</sub>	HT-CO <sub>2</sub>	BT-CO <sub>2</sub>	HT-CO <sub>2</sub>
PFO	$q_e$ (mg g <sup>-1</sup> )	51.71	86.55	31.51	59.60
	$k_1$ (min <sup>-1</sup> )	0.195	0.324	0.346	0.276
	$R_2$	0.796	0.915	0.969	0.934
PSO	$q_e$ (mg g <sup>-1</sup> )	54.41	89.06	32.13	61.36
	$k_2$ (min <sup>-1</sup> )	$4.08 \times 10^{-3}$	$5.76 \times 10^{-3}$	0.0220	$7.24 \times 10^{-3}$
	$R_2$	0.882	0.952	0.988	0.973
Elovich	$\alpha$ (mg g <sup>-1</sup> min <sup>-1</sup> )	2503.6	7417.6	18,237.3	98,117.6
	$\beta$ (mg g <sup>-1</sup> )	0.236	0.232	0.933	0.351
	$R_2$	0.990	0.997	0.997	0.992

### 3.3. Batch Adsorption Isotherm

The experimental data obtained from the acetaminophen and caffeine adsorption isotherm tests by BT-CO<sub>2</sub> and HT-CO<sub>2</sub> are shown in Figure 4C and 4D, respectively. The maximum acetaminophen adsorption capacities ( $q_{max}$ ) were 221.4 and 383.2 mg g<sup>-1</sup> for BT-CO<sub>2</sub> and HT-CO<sub>2</sub>, respectively. For caffeine, they were 162.7 and 189.7 mg g<sup>-1</sup> for BT-CO<sub>2</sub> and HT-CO<sub>2</sub>, respectively.

Analyzing the equilibrium data, these were adjusted to three theoretical models: Langmuir, Freundlich, and BET. The parameter results for each model are compiled in Table 4. It is observed that the Langmuir and BET models presented the best fit for the adsorption of paracetamol by BT-CO<sub>2</sub> and HT-CO<sub>2</sub>, respectively. As for caffeine adsorption, the Langmuir model proved to be more suitable for describing the experimental data for both BT-CO<sub>2</sub> and HT-CO<sub>2</sub>.

**Table 4.** Modeling parameters of the BT-CO<sub>2</sub> and HT-CO<sub>2</sub> adsorption isotherms.

Model	Parameter	Acetaminophen		Caffeine	
		BT-CO <sub>2</sub>	HT-CO <sub>2</sub>	BT-CO <sub>2</sub>	HT-CO <sub>2</sub>
Langmuir	$q_{max}$ (mg g <sup>-1</sup> )	240.86	2822.23	168.68	185.22
	$K_L$ (L mg <sup>-1</sup> )	$2.14 \times 10^{-3}$	$1.60 \times 10^{-4}$	$2.27 \times 10^{-3}$	0.0127
	$R_2$	0.983	0.739	0.988	0.978
Freundlich	$K_F$ (mg g <sup>-1</sup> )/(L mg <sup>-1</sup> ) <sup>1/n</sup>	4.61	4.28	3.34	22.30
	$n$	1.68	1.59	1.68	3.30
	$R_2$	0.974	0.787	0.965	0.965
BET	$q_m$ (mg g <sup>-1</sup> )	86.30	88.57	65.04	88.67
	$K_s$ (L mg <sup>-1</sup> )	$6.63 \times 10^{43}$	8.08	$3.10 \times 10^{45}$	$1.62 \times 10^{43}$
	$K_L$ (L mg <sup>-1</sup> )	$8.50 \times 10^{-4}$	$9.5 \times 10^{-4}$	$8.00 \times 10^{-4}$	$6.3 \times 10^{-4}$
	$R_2$	0.755	0.970	0.729	0.771

The Langmuir model describes adsorption on the surface of the adsorbent as homogeneous and monolayer, so the active sites are similar and have the same affinity for the adsorbate in question, with no lateral or steric interaction. Furthermore, adsorption, in this case, is irreversible [36]. On the other hand, the BET isotherm describes multilayer adsorption, where adsorption first occurs through adsorbate–adsorbent interactions until the monolayer is saturated. Then, the adsorbate can interact with other previously adsorbed molecules to form a new layer [15].

As HT-CO<sub>2</sub> showed a higher adsorption capacity for acetaminophen and caffeine than BT-CO<sub>2</sub>, the maximum adsorption ( $q_m$ , experimental) capacity of HT-CO<sub>2</sub> was compared with that of other adsorbents (see Table 5). According to the results shown in Table 4, HT-CO<sub>2</sub> has enormous potential to be used in water treatment processes that contain acetaminophen and caffeine.

**Table 5.** Maximum acetaminophen and caffeine adsorption capacities in different adsorbents.

Adsorbent	Experimental Conditions					$q_m$ , experimental (mg g <sup>-1</sup> )	Reference
	T (°C)	Mass (mg)	Time (min)	C <sub>initial</sub> (mg L <sup>-1</sup> )	Contaminant		
Corn cob biochar	-	1000	360	0–500	Acetaminophen	64.9	[37]
Walnut shell	-	100	120	5–80	Acetaminophen	15.3	[38]
Biobased carbon material activated with ZnSO <sub>4</sub>	23	30	2	70–1200	Acetaminophen	364.8	[33]
Biobased carbon material activated with MgCl <sub>2</sub>	23	30	4	70–1200	Acetaminophen	321.2	[33]
Banana peel	45	2000	1500	0–200	Acetaminophen	57.3	[39]
Brewer’s spent grain	30	25	60	100–1000	Acetaminophen	318.0	[40]
Norway spruce (Picea abies) needles	25	10	300	10–40	Caffeine	9.2	[40]
Pine (Pinus strobus) needles	25	10	300	10–40	Caffeine	11.9	[41]
Mangium acacia wood	25	3000	61	0–100	Caffeine	29.2	[42]
Macrophyte (Eichornia crassipes)	25	25	50	25–500	Caffeine	112.7	[43]
BT-CO <sub>2</sub>	25	20	1440	25–1000	Acetaminophen	383.2	This work
BT-CO <sub>2</sub>	25	20	1440	25–1000	Caffeine	189.7	This work

### 3.4. Fixed Bed Column Adsorption Experiments

Given the best performance of the HT-CO<sub>2</sub> sample in adsorbing both adsorbate molecules, fixed-bed experiments were carried out only with this adsorbent. The break-through curve of effluent concentration ( $C/C_0$ ) versus time and the mathematical modeling of acetaminophen and caffeine adsorption on HT-CO<sub>2</sub> are presented in Figure 5, while column performance data are shown in Table 6. The maximum adsorption capacity of acetaminophen and caffeine by HT-CO<sub>2</sub> was 82.23 and 45.60 mg g<sup>-1</sup>, respectively.

**Table 6.** Thomas, Adams–Bohart, Yoon–Nelson, dose–response model parameters using HT-CO<sub>2</sub>.

Model	Parameter	Acetaminophen	Caffeine
		m = 0.2 g Q = 3 mL min <sup>-1</sup> C <sub>0</sub> = 25 mg L <sup>-1</sup> Z = 2.1 cm t <sub>r</sub> (C <sub>t</sub> /C <sub>0</sub> = 0.05) = 70.2 min t <sub>s</sub> (C <sub>t</sub> /C <sub>0</sub> = 0.94) = 491.6 min ZTM = 1.80 cm V <sub>efflu</sub> = 1474.8 mL m <sub>DIC_total</sub> = 36.87 mg m <sub>DIC_ads</sub> = 16.44 mg q <sub>total</sub> = 82.23 mg g <sup>-1</sup> %R = 44.6%	m = 0.2 g Q = 3 mL min <sup>-1</sup> C <sub>0</sub> = 25 mg L <sup>-1</sup> Z = 2.1 cm t <sub>r</sub> (C <sub>t</sub> /C <sub>0</sub> = 0.05) = 5.6 min t <sub>s</sub> (C <sub>t</sub> /C <sub>0</sub> = 0.94) = 415.9 min ZTM = 2.1 cm V <sub>efflu</sub> = 1247.7 mL m <sub>DIC_total</sub> = 31.2 mg m <sub>DIC_ads</sub> = 9.1 mg q <sub>total</sub> = 45.6 mg g <sup>-1</sup> %R = 20.0%

Table 6. Cont.

Thomas	$k_{Th}$ (L mg <sup>-1</sup> min <sup>-1</sup> )	$5.9 \times 10^{-4}$	$6.6 \times 10^{-4}$
	$q_0$ (mg g <sup>-1</sup> )	79.7	36.7
	$R^2$	0.986	0.952
Adams-Bohart	$k_{AB}$ (L mg <sup>-1</sup> min <sup>-1</sup> )	$5.90 \times 10^{-4}$	$6.6 \times 10^{-4}$
	$N_0$ (mg L <sup>-1</sup> )	54,889.0	27,731.6
	$R^2$	0.986	0.952
Yoon-Nelson	$k_{YN}$ (min <sup>-1</sup> )	0.0146	0.0165
	$\tau_{cal}$ (min)	212.5	97.8
	$R^2$	0.986	0.952
Dose-response	$\alpha$	2.80	1.56
	$q_0$ (mg g <sup>-1</sup> )	75.0	30.8
	$R^2$	0.997	0.986

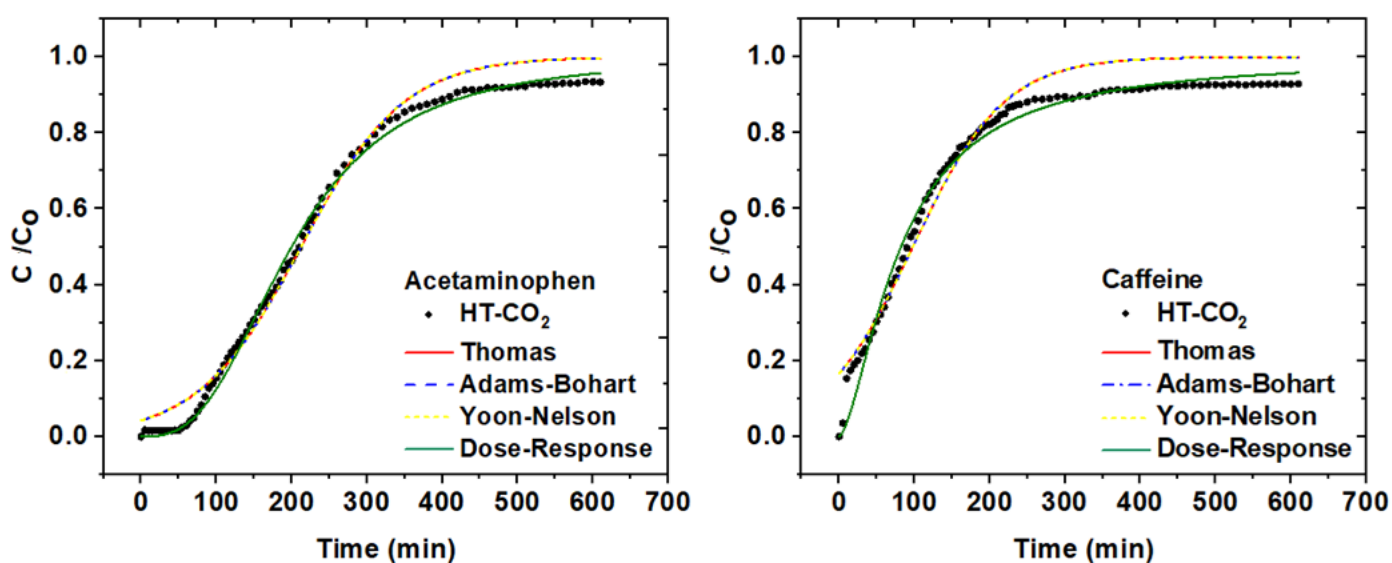


Figure 5. Breakthrough curves with mathematical modelling of adsorption of acetaminophen and caffeine onto HT-CO<sub>2</sub>.

Figure 5 shows that the breakthrough curve for caffeine was not as S-shaped (symmetrical) as for acetaminophen. This indicates that there were dispersion effects in the caffeine breakthrough curve. Dispersion effects arise from the non-ideal packing of the column, axial dispersion, resistance to mass transfer, and the distribution of fluids along the column [44,45].

The effects of dispersion are also reflected in the results of the mass transfer zone (MTZ) and, consequently, in the breakthrough time ( $t_r$ ) and saturation time ( $t_s$ ). The data presented in Table 6 shows that the mass transfer zone (MTZ) was smaller and the breakthrough and saturation times were longer for acetaminophen compared to the values obtained in the caffeine removal test. These results are consistent with the fact that HT-CO<sub>2</sub> has a higher adsorption capacity for acetaminophen than for caffeine, since the lower the dispersion effects, the greater the adsorption capacity of contaminants by the adsorbent material. Furthermore, longer breakthrough and saturation times mean longer contact between the contaminant molecules and the column’s adsorbent bed [46].

Regarding the column performance data in Table 6, the dose-response model best fits the experimental data on removing paracetamol and caffeine by HT-CO<sub>2</sub>. The dose-response model is applied to estimate the adsorptive capacity of the adsorbent. This model suggests that the increase in  $q_{total}$  is directly related to the amount of adsorbent material, surface area, and residence time. In addition, low values of the  $\alpha$  and  $q_0$  parameters

indicate increased mass transport resistance [47]. It should be noted that all these facts were observed in the results of the fixed-bed experiments.

### 3.5. Adsorption Mechanism of Acetaminophen and Caffeine

The capture of organic pollutants by carbon-based adsorbents generally occurs through several mechanisms, such as electrostatic attraction, Van der Waals forces, ion exchange, formation of hydrogen bonds,  $\pi$ - $\pi$  interactions, and pore filling [48]. In the present study, mechanisms such as pore filling, hydrogen bonds, and dipole-dipole interactions were shown to be crucial for the adsorption of paracetamol and caffeine by BT-CO<sub>2</sub> and HT-CO<sub>2</sub>.

The electron donor-acceptor mechanism, also known as  $\pi$ - $\pi$  interaction, involves the transfer of electrons between oxygen carbonyl ions on the surface of the adsorbent, which acts as a donor, and the aromatic ring structure of the adsorbate, which acts as an acceptor [49].

The hydrogen bond, responsible for the interaction between adsorbent and adsorbate, can be established in two ways: dipole-dipole or Yoshida. In the dipole-dipole mechanism, the hydrogen of the hydroxyl group on the surface of the adsorbent binds to suitable atoms (oxygen and nitrogen) in the aromatic structure of the adsorbate. In the Yoshida hydrogen bond, the interaction takes place between the aromatic ring of the adsorbate and the hydroxyl groups on the surface of the adsorbent [50].

Similar adsorption mechanisms to those observed in this study were proposed by [51,52] for acetaminophen removal and [53,54] for caffeine removal.

## 4. Conclusions

This study examined the adsorption efficacy of CO<sub>2</sub>-activated biochar (BT-CO<sub>2</sub>) and CO<sub>2</sub>-activated hydrochar (HT-CO<sub>2</sub>) in removing paracetamol and caffeine from aqueous solutions in batch and fixed-bed systems. In batch systems, HT-CO<sub>2</sub> demonstrated significantly higher efficiency in adsorbing paracetamol and caffeine than BT-CO<sub>2</sub>. BT-CO<sub>2</sub> exhibited a maximum adsorption capacity of 221.4 mg g<sup>-1</sup> for paracetamol and 162.7 mg g<sup>-1</sup> for caffeine, whereas HT-CO<sub>2</sub> showed superior capacities of 383.2 mg g<sup>-1</sup> for paracetamol and 189.7 mg g<sup>-1</sup> for caffeine. Conversely, in fixed-bed systems, HT-CO<sub>2</sub> displayed a greater capacity for paracetamol removal than for caffeine, with maximum adsorption capacities of 82.2 mg g<sup>-1</sup> and 45.6 mg g<sup>-1</sup>, respectively. The adsorption process for both compounds was predominantly governed by physical mechanisms such as hydrogen bonding (H) and  $\pi$ - $\pi$  interactions involving functional groups on the adsorbent material surface and the adsorbed molecules. These findings highlight the potential of HT-CO<sub>2</sub> as a promising alternative adsorbent for effectively removing paracetamol from water sources. Desorption/regeneration assays will be addressed in future work, since it is crucial to manage the saturated adsorbent through reuse or safe disposal.

**Author Contributions:** D.d.S.—Methodology, Investigation, Writing—Original Draft. W.M.—Methodology, Investigation, Writing—Original Draft. T.d.A.—Data Curation, Writing—Original Draft. M.B.—Investigation, Writing—Review and Editing. I.F.—Writing—Review and Editing. I.O.—Resources, Writing—Review and Editing, Supervision. M.A.d.B.—Resources, Writing—Review and Editing, Supervision, Project Administration. All authors have read and agreed to the published version of the manuscript.

**Funding:** This study was partly funded by the National Council for Scientific and Technological Development—CNPq (Process 200678/2022-1). It also received financial support from FCT/MCTES (UIDP/50006/2020 DOI 10.54499/UIDP/50006/2020) through national (Portuguese) funds.

**Data Availability Statement:** The original contributions presented in the study are included in the article, further inquiries can be directed to the corresponding authors.

**Conflicts of Interest:** The authors declare no conflicts of interest.

## References

1. Graham, G.G.; Davies, M.J.; Day, R.O.; Mohamudally, A.; Scott, K.F. The Modern Pharmacology of Paracetamol: Therapeutic Actions, Mechanism of Action, Metabolism, Toxicity and Recent Pharmacological Findings. *Inflammopharmacology* **2013**, *21*, 201–232. [[CrossRef](#)] [[PubMed](#)]
2. Starling-Soares, B.; Pereira, M.; Renke, G. Extrapolating the Coffee and Caffeine (1,3,7-Trimethylxanthine) Effects on Exercise and Metabolism—A Concise Review. *Nutrients* **2023**, *15*, 5031. [[CrossRef](#)] [[PubMed](#)]
3. Shaheen, J.F.; Sizirici, B.; Yildiz, I. Fate, Transport, and Risk Assessment of Widely Prescribed Pharmaceuticals in Terrestrial and Aquatic Systems: A Review. *Emerg. Contam.* **2022**, *8*, 216–228. [[CrossRef](#)]
4. De Cravalho, A.C.C.; da Silva Paganini, W.; de Almeida Piai, K.; Bocchiglieri, M.M. The Presence of Pharmaceuticals and Caffeine in Water, as Well as the Methods Used to Eliminate Them. *Curr. Opin. Environ. Sci. Health* **2024**, *39*, 100550. [[CrossRef](#)]
5. Quadra, G.R.; Oliveira de Souza, H.; Costa, R.d.S.; Fernandez, M.A.d.S. Do Pharmaceuticals Reach and Affect the Aquatic Ecosystems in Brazil? A Critical Review of Current Studies in a Developing Country. *Environ. Sci. Pollut. Res.* **2017**, *24*, 1200–1218. [[CrossRef](#)] [[PubMed](#)]
6. Ghosh, R.; Parde, D.; Bhaduri, S.; Rajpurohit, P.; Behera, M. Occurrence, Fate, Transport, and Removal Technologies of Emerging Contaminants: A Review on Recent Advances and Future Perspectives. *Clean-Soil Air Water* **2024**, *52*, 2300259. [[CrossRef](#)]
7. Ullah, S.; Shah, S.S.A.; Altaf, M.; Hossain, I.; El Sayed, M.E.; Kallel, M.; El-Bahy, Z.M.; Rehman, A.U.; Najam, T.; Nazir, M.A. Activated Carbon Derived from Biomass for Wastewater Treatment: Synthesis, Application and Future Challenges. *J. Anal. Appl. Pyrolysis* **2024**, *179*, 106480. [[CrossRef](#)]
8. Akintola, A.T.; Ayankunle, A.Y. Improving Pharmaceuticals Removal at Wastewater Treatment Plants Using Biochar: A Review. *Waste Biomass Valorization* **2023**, *14*, 2433–2458. [[CrossRef](#)]
9. Tolkou, A.K.; Maroulas, K.N.; Theologis, D.; Katsoyiannis, I.A.; Kyzas, G.Z. Comparison of Modified Peels: Natural Peels or Peels-Based Activated Carbons for the Removal of Several Pollutants Found in Wastewaters. *C-J. Carbon. Res.* **2024**, *10*, 22. [[CrossRef](#)]
10. Sharma, H.B.; Vanapalli, K.R.; Bhatia, D.; Singh, S.; Arora, G.; Panigrahi, S.; Dubey, B.K.; Ramamurthy, P.C.; Mohanty, B. *Engineered Biochar/Hydrochar Derived from Organic Wastes for Energy, Environmental, and Agricultural Applications*; Springer: Berlin/Heidelberg, Germany, 2024; ISBN 1009802402.
11. Moraes, A.R.A.; Camargo, K.C.; Simões, M.O.M.; Ferraz, V.P.; Pereira, M.T.; Evangelista, F.C.G.; Sabino, A.P.; Duarte, L.P.; Alcântara, A.F.C.; de Sousa, G.F. Chemical Composition of *Magonia pubescens* Essential Oils and Gamma-Radiation Effects on Its Constituents and Cytotoxic Activity in Leukemia and Breast Cancer Model. *Chem. Biodivers.* **2021**, *18*, e2100094. [[CrossRef](#)]
12. Moraes, A.R.A.; Sabina, S.R.; Expósito, D.G.; Giménez, C.; Espinel, G.; Sousa, G.F.; Duarte, L.P.; Jiménez, I.A.; Cabrera, R.; Bazzocchi, I.L. Evaluation of *Magonia pubescens* A. St.-Hill. Roots Extract against Phytopathogens: Searching for Eco-Friendly Crop Protection Products. *Appl. Sci.* **2023**, *13*, 6736. [[CrossRef](#)]
13. Moraes, A.R.A.; Siqueira, E.P.; Kohlhoff, M.; Evangelista, F.C.G.; Sabino, A.P.; Vieira Filho, S.A.; Alcântara, A.F.C.; Duarte, L.P.; Sousa, G.F. Phytochemical Study of *Magonia pubescens* A. St.-Hil. and Cytotoxicity of Branches Aqueous Extract on Breast Cancer and Leukemia Cells. *Nat. Prod. Res.* **2024**, *38*, 1956–1960. [[CrossRef](#)] [[PubMed](#)]
14. Dos Santos, D.F.; Moreira, W.M.; de Araújo, T.P.; Bernardo, M.M.S.; de Figueiredo Ligeiro da Fonseca, I.M.; Ostroski, I.C.; de Barros, M.A.S.D. Competitive Adsorption of Acetaminophen and Caffeine onto Activated *Tingui* Biochar: Characterization, Modeling, and Mechanisms. *Environ. Sci. Pollut. Res.* **2023**. [[CrossRef](#)] [[PubMed](#)]
15. Federici dos Santos, D.; Moreira, W.M.; de Araújo, T.P.; Martins, D.C.C.; Carvalho da Silva Fonseca, B.; Ostroski, I.C.; de Barros, M.A.S.D. Novel Activated Carbon from *Magonia pubescens* Bark: Characterization and Evaluation of Adsorption Efficiency. *Environ. Technol.* **2023**. [[CrossRef](#)] [[PubMed](#)]
16. EN 15290:2011; Air Quality—Determination of Major and Trace Elements in Ambient Air—Inductively Coupled Plasma Mass Spectrometric (ICP-MS) Method. European Committee for Standardization (CEN): Brussels, Belgium, 2011.
17. Ho, Y.S.; McKay, G. A Comparison of Chemisorption Kinetic Models Applied to Pollutant Removal on Various Sorbents. *Process Saf. Environ. Prot.* **1998**, *76*, 332–340. [[CrossRef](#)]
18. Febrianto, J.; Kosasih, A.N.; Sunarso, J.; Ju, Y.H.; Indraswati, N.; Ismadi, S. Equilibrium and Kinetic Studies in Adsorption of Heavy Metals Using Biosorbent: A Summary of Recent Studies. *J. Hazard. Mater.* **2009**, *162*, 616–645. [[CrossRef](#)] [[PubMed](#)]
19. Chatterjee, A.; Schiewer, S. Biosorption of Cadmium(II) Ions by Citrus Peels in a Packed Bed Column: Effect of Process Parameters and Comparison of Different Breakthrough Curve Models. *CLEAN—Soil Air Water* **2011**, *39*, 874–881. [[CrossRef](#)]
20. Yan, S.; Qu, J.; Bi, F.; Wei, S.; Wang, S.; Jiang, Z.; Wang, L.; Yu, H.; Zhang, Y. One-Pot Synthesis of Porous N-Doped Hydrochar for Atrazine Removal from Aqueous Phase: Co-Activation and Adsorption Mechanisms. *Bioresour. Technol.* **2022**, *364*, 128056. [[CrossRef](#)] [[PubMed](#)]
21. Vandeponsele, A.; Draye, M.; Piot, C.; Chatel, G. Study of Influential Parameters of the Caffeine Extraction from Spent Coffee Grounds: From Brewing Coffee Method to the Waste Treatment Conditions. *Clean. Technol.* **2021**, *3*, 335–350. [[CrossRef](#)]
22. Bursztyn Fuentes, A.L.; Benito, D.E.; Montes, M.L.; Scian, A.N.; Lombardi, M.B. Paracetamol and Ibuprofen Removal from Aqueous Phase Using a Ceramic-Derived Activated Carbon. *Arab. J. Sci. Eng.* **2023**, *48*, 525–537. [[CrossRef](#)]
23. Álvarez-Murillo, A.; Ledesma, B.; Román, S.; Sabio, E.; Gañán, J. Biomass Pyrolysis toward Hydrocarbonization. Influence on Subsequent Steam Gasification Processes. *J. Anal. Appl. Pyrolysis* **2015**, *113*, 380–389. [[CrossRef](#)]



24. Kambo, H.S.; Dutta, A. A Comparative Review of Biochar and Hydrochar in Terms of Production, Physico-Chemical Properties and Applications. *Renew. Sustain. Energy Rev.* **2015**, *45*, 359–378. [[CrossRef](#)]
25. Yang, J.; Zhang, Z.; Wang, J.; Zhao, X.; Zhao, Y.; Qian, J.; Wang, T. Pyrolysis and Hydrothermal Carbonization of Biowaste: A Comparative Review on the Conversion Pathways and Potential Applications of Char Product. *Sustain. Chem. Pharm.* **2023**, *33*, 101106. [[CrossRef](#)]
26. Silva, J.O.S.; Granja, H.S.; dos Santos, J.F.; Freitas, L.S.; Sussuchi, E.M. Biochar and Hydrochar in the Development and Application of Electrochemical Devices in the Sensing and Degradation of Target Compounds: A Mini-Review of the Recent Contributions of 2020–2023. *J. Braz. Chem. Soc.* **2024**, *35*, 1–18. [[CrossRef](#)]
27. Thommes, M.; Kaneko, K.; Neimark, A.V.; Olivier, J.P.; Rodriguez-Reinoso, F.; Rouquerol, J.; Sing, K.S.W. IUPAC Technical Report Physisorption of Gases, with Special Reference to the Evaluation of Surface Area and Pore Size Distribution (IUPAC Technical Report). *Pure Appl. Chem.* **2015**, *87*, 1051–1069. [[CrossRef](#)]
28. Kinashi, K.; Kambe, Y.; Misaki, M.; Koshihara, Y.; Ishida, K.; Ueda, Y. Synthesis, Characterization, Photo-Induced Alignment, and Surface Orientation of Poly(9,9-Dioctylfluorene-Alt-Azobenzene)S. *J. Polym. Sci. Part. A Polym. Chem.* **2012**, *50*, 5107–5114. [[CrossRef](#)]
29. Tian, X.-L.; Yu, J.-H.; Qiu, L.; Zhu, Y.-H.; Zhu, M.-Q. Structural Changes and Electrochemical Properties of Mesoporous Activated Carbon Derived from *Eucommia Ulmoides* Wood Tar by KOH Activation for Supercapacitor Applications. *Ind. Crops Prod.* **2023**, *197*, 116628. [[CrossRef](#)]
30. Karakehya, N. Effects of One-Step and Two-Step KOH Activation Method on the Properties and Supercapacitor Performance of Highly Porous Activated Carbons Prepared from *Lycopodium clavatum* Spores. *Diam. Relat. Mater.* **2023**, *135*, 109873. [[CrossRef](#)]
31. Aziz, S.; Uzair, B.; Ali, M.I.; Anbreen, S.; Umer, F.; Khalid, M.; Aljabali, A.A.; Mishra, Y.; Mishra, V.; Serrano-Aroca, Á.; et al. Synthesis and characterization of nanobiochar from rice husk biochar for the removal of safranin and malachite green from water. *Environ. Res.* **2023**, *238*, 116909. [[CrossRef](#)]
32. Hamissou, I.G.M.; Appiah, K.E.K.; Sylvie, K.A.T.; Ousmaila, S.M.; Casimir, B.Y.; Benjamin, Y.K. Valorization of Cassava Peelings into Biochar: Physical and Chemical Characterizations of Biochar Prepared for Agricultural Purposes. *Sci. Afr.* **2023**, *20*, e01737. [[CrossRef](#)]
33. Dos Reis, G.S.; Guy, M.; Mathieu, M.; Jebrane, M.; Lima, E.C.; Thyrel, M.; Dotto, G.L.; Larsson, S.H. A Comparative Study of Chemical Treatment by MgCl<sub>2</sub>, ZnSO<sub>4</sub>, ZnCl<sub>2</sub>, and KOH on Physicochemical Properties and Acetaminophen Adsorption Performance of Biobased Porous Materials from Tree Bark Residues. *Colloids Surf. A Physicochem. Eng. Asp.* **2022**, *642*, 128626. [[CrossRef](#)]
34. Machado, T.S.; Crestani, L.; Marchezi, G.; Melara, F.; de Mello, J.R.; Dotto, G.L.; Piccin, J.S. Synthesis of Glutaraldehyde-Modified Silica/Chitosan Composites for the Removal of Water-Soluble Diclofenac Sodium. *Carbohydr. Polym.* **2022**, *277*, 118868. [[CrossRef](#)] [[PubMed](#)]
35. Zhang, X.; Zhang, J.; She, Y.; Li, Y.; Cheng, H.; Ji, R.; Bian, Y.; Han, J.; Jiang, X.; Song, Y.; et al. Comparison of the Performance of Hydrochar, Raw Biomass, and Pyrochar as Precursors to Prepare Porous Biochar for the Efficient Sorption of Phthalate Esters. *Sci. Total Environ.* **2022**, *846*, 157511. [[CrossRef](#)] [[PubMed](#)]
36. Pimentel-Almeida, W.; Itokazu, A.G.; Bazani, H.A.G.; Maraschin, M.; Rodrigues, O.H.C.; Corrêa, R.G.; Lopes, S.; Almerindo, G.I.; Moresco, R. Beach-Cast *Sargassum cymosum* Macroalgae: Biochar Production and Apply to Adsorption of Acetaminophen in Batch and Fixed-Bed Adsorption Processes. *Environ. Technol.* **2023**, *44*, 974–987. [[CrossRef](#)] [[PubMed](#)]
37. Varela, C.F.; Moreno-Aldana, L.C.; Agámez-Pertuz, Y.Y. Adsorption of Pharmaceutical Pollutants on ZnCl<sub>2</sub>-Activated Biochar from Corn Cob: Efficiency, Selectivity and Mechanism. *J. Bioresour. Bioprod.* **2023**, *9*, 58–73. [[CrossRef](#)]
38. Turcanu, A.A.; Matei, E.; Răpă, M.; Predescu, A.M.; Berbecaru, A.C.; Coman, G.; Predescu, C. Walnut Shell Biowaste Valorization via HTC Process for the Removal of Some Emerging Pharmaceutical Pollutants from Aqueous Solutions. *Int. J. Mol. Sci.* **2022**, *23*, 11095. [[CrossRef](#)]
39. Patel, M.; Kumar, R.; Pittman, C.U.; Mohan, D. Ciprofloxacin and Acetaminophen Sorption onto Banana Peel Biochars: Environmental and Process Parameter Influences. *Environ. Res.* **2021**, *201*, 111218. [[CrossRef](#)]
40. De Araújo, T.P.; Quesada, H.B.; Bergamasco, R.; Vareschini, D.T.; de Barros, M.A.S.D. Activated Hydrochar Produced from Brewer's Spent Grain and Its Application in the Removal of Acetaminophen. *Bioresour. Technol.* **2020**, *310*, 123399. [[CrossRef](#)]
41. Oginni, O.; Singh, K. Effect of Carbonization Temperature on Fuel and Caffeine Adsorption Characteristics of White Pine and Norway Spruce Needle Derived Biochars. *Ind. Crops Prod.* **2021**, *162*, 113261. [[CrossRef](#)]
42. Danish, M.; Birnbach, J.; Mohamad Ibrahim, M.N.; Hashim, R.; Majeed, S.; Tay, G.S.; Sapawe, N. Optimization Study of Caffeine Adsorption onto Large Surface Area Wood Activated Carbon through Central Composite Design Approach. *Environ. Nanotechnol. Monit. Manag.* **2021**, *16*, 100594. [[CrossRef](#)]
43. Zanella, H.G.; Spessato, L.; Lopes, G.K.P.; Yokoyama, J.T.C.; Silva, M.C.; Souza, P.S.C.; Ronix, A.; Cazetta, A.L.; Almeida, V.C. Caffeine Adsorption on Activated Biochar Derived from Macrophytes (*Eichornia crassipes*). *J. Mol. Liq.* **2021**, *340*, 117206. [[CrossRef](#)]
44. De Araujo, C.M.B.; Wernke, G.; Ghislandi, M.G.; Diório, A.; Vieira, M.F.; Bergamasco, R.; Alves da Motta Sobrinho, M.; Rodrigues, A.E. Continuous Removal of Pharmaceutical Drug Chloroquine and Safranin-O Dye from Water Using Agar-Graphene Oxide Hydrogel: Selective Adsorption in Batch and Fixed-Bed Experiments. *Environ. Res.* **2023**, *216*, 114425. [[CrossRef](#)] [[PubMed](#)]

45. De Araujo, C.M.B.; Ghislandi, M.G.; Rios, A.G.; da Costa, G.R.B.; do Nascimento, B.F.; Ferreira, A.F.P.; da Motta Sobrinho, M.A.; Rodrigues, A.E. Wastewater Treatment Using Recyclable Agar-Graphene Oxide Biocomposite Hydrogel in Batch and Fixed-Bed Adsorption Column: Bench Experiments and Modeling for the Selective Removal of Organics. *Colloids Surf. A Physicochem. Eng. Asp.* **2022**, *639*, 128357. [[CrossRef](#)]
46. Silveira Neto, A.L.; Pimentel-Almeida, W.; Niero, G.; Wanderlind, E.H.; Radetski, C.M.; Almerindo, G.I. Application of a Biochar Produced from Malt Bagasse as a Residue of Brewery Industry in Fixed-Bed Column Adsorption of Paracetamol. *Chem. Eng. Res. Des.* **2023**, *194*, 779–786. [[CrossRef](#)]
47. Tejedor, J.; Álvarez-Briceño, R.; Guerrero, V.H.; Villamar-Ayala, C.A. Removal of Caffeine Using Agro-Industrial Residues in Fixed-Bed Columns: Improving the Adsorption Capacity and Efficiency by Selecting Adequate Physical and Operational Parameters. *J. Water Process Eng.* **2023**, *53*, 103778. [[CrossRef](#)]
48. Pauletto, P.S.; Lütke, S.F.; Dotto, G.L.; Salau, N.P.G. Adsorption Mechanisms of Single and Simultaneous Removal of Pharmaceutical Compounds onto Activated Carbon: Isotherm and Thermodynamic Modeling. *J. Mol. Liq.* **2021**, *336*, 116203. [[CrossRef](#)]
49. Tran, H.N.; Tomul, F.; Thi Hoang Ha, N.; Nguyen, D.T.; Lima, E.C.; Le, G.T.; Chang, C.T.; Masindi, V.; Woo, S.H. Innovative Spherical Biochar for Pharmaceutical Removal from Water: Insight into Adsorption Mechanism. *J. Hazard. Mater.* **2020**, *394*, 122255. [[CrossRef](#)]
50. Islam, A.; Nazal, M.K.; Sajid, M.; Suliman, M.A. Adsorptive Removal of Paracetamol from Aqueous Media: A Review of Adsorbent Materials, Adsorption Mechanisms, Advancements, and Future Perspectives. *J. Mol. Liq.* **2024**, *396*, 123976. [[CrossRef](#)]
51. Geczo, A.; Giannakoudakis, D.A.; Triantafyllidis, K.; Elshaer, M.R.; Rodríguez-Aguado, E.; Bashkova, S. Mechanistic Insights into Acetaminophen Removal on Cashew Nut Shell Biomass-Derived Activated Carbons. *Environ. Sci. Pollut. Res.* **2021**, *28*, 58969–58982. [[CrossRef](#)]
52. El Saied, M.; Seham, S.A.; Shaban, A.; Mohsen, M.S.; Mostafa, S.; Abo, A.O.; Naga, E. Efficient Adsorption of Acetaminophen from the Aqueous Phase Using Low-Cost and Renewable Adsorbent Derived from Orange Peels. *Biomass Convers. Biorefinery* **2022**, *14*, 2155–2172. [[CrossRef](#)]
53. Francoeur, M.; Ferino-Pérez, A.; Yacou, C.; Jean-Marius, C.; Emmanuel, E.; Chérémond, Y.; Jauregui-Haza, U.; Gaspard, S. Activated Carbon Synthesized from *Sargassum* (Sp) for Adsorption of Caffeine: Understanding the Adsorption Mechanism Using Molecular Modeling. *J. Environ. Chem. Eng.* **2021**, *9*, 104795. [[CrossRef](#)]
54. Bachmann, S.A.L.; Calvete, T.; Féris, L.A. Caffeine Removal from Aqueous Media by Adsorption: An Overview of Adsorbents Evolution and the Kinetic, Equilibrium and Thermodynamic Studies. *Sci. Total Environ.* **2021**, *767*, 144229. [[CrossRef](#)] [[PubMed](#)]

**Disclaimer/Publisher's Note:** The statements, opinions and data contained in all publications are solely those of the individual author(s) and contributor(s) and not of MDPI and/or the editor(s). MDPI and/or the editor(s) disclaim responsibility for any injury to people or property resulting from any ideas, methods, instructions or products referred to in the content.